Dynamic wetting behavior on oxidized surfaces and its effect on pool boiling critical heat flux

Namgook Kim[1], Hong Hyun Son[1], Sung Joong Kim[1,2*]
[1]*Department of Nuclear Engineering, Hanyang University*
[2]*Institute of Nano Science & Technology, Hanyang University*
222 Wangsimri-ro, Seongdong-gu, Seoul 04763, Republic of Korea
ngkim@hanyang.ac.kr, hhson@hanyang.ac.kr,
[*]*Corresponding author: sungjkim@hanyang.ac.kr*

1. Introduction

Critical heat flux (CHF) is an important criterion in nuclear reactor safety and the efficiency of boiling heat transfer. This parameter is known to be dependent of the surface roughness and the wettability of a material that is in contact with boiling fluid. Generally, CHF enhances with increasing surface roughness and wettability. However, the uncombined effect of each dependency is not yet well understood. One way to better understand this is to analyze the dynamic wetting behavior. Thus this study reports the effect of dynamic wetting behavior on CHF using oxidized steel samples to modify roughness and wettability.

2. Experiment

2.1 Sample preparation

Grade 304 stainless steel samples were used in the study. The samples were ground with grade-800 and -320 sandpapers and cleansed with an ethanol solution to remove any contaminants. Later, the samples were oxidized in a furnace under dry air condition. The adopted temperature conditions and oxidation times are listed in Table 1. After oxidation, the samples were characterized with scanning electron microscopy (SEM).

Table 1. Oxidation condition

Oxidation parameter	Oxidation condition I	Oxidation condition II
Surface material	Stainless steel grade 304 plate	Stainless steel grade 304 plate
Temperature (°C)	500	700
Time (days)	10	3

2.2 Experimental setup

A schematic of the pool boiling experimental apparatus and a design of the test section used in the study are shown in Fig. 1. The length, width, and thickness of test material were 45, 10, and 2 mm, respectively. Heat transfer surface area was 25×10 = 250 mm^2 because rest 10 mm of both sides were connected with copper electrodes and copper cover for electrical contact. Polyether ether ketone (PEEK) and epoxy were used for thermal and electrical insulation. A K-type thermocouple was attached underneath the samples to measure inner wall temperature (Fig. 1 (c)). Voltage taps were attached to the PEEK screw at each side to measure voltage drop.

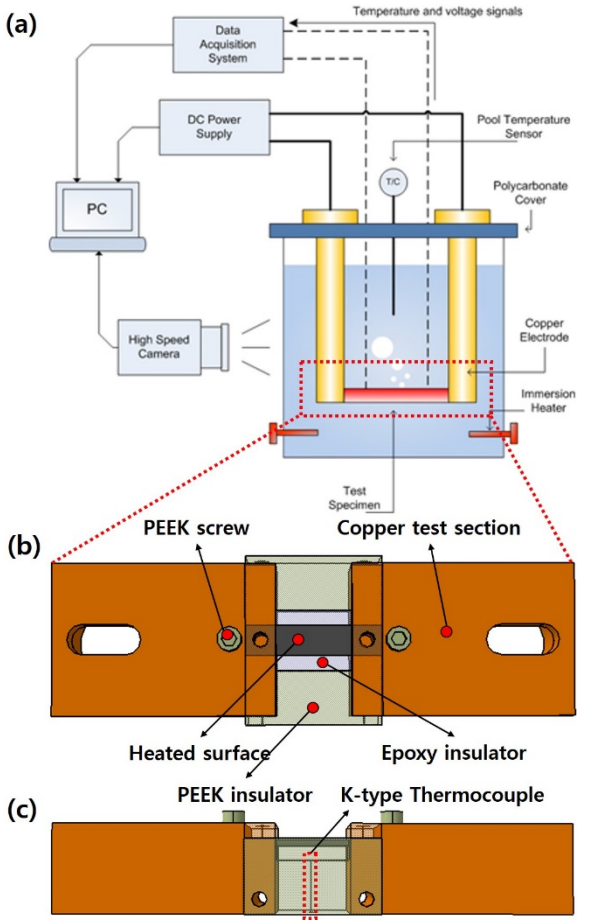

Fig. 1. Schematic diagram of (a) pool boiling apparatus; (b) upper side test section; (c) lateral side test section.

Direct Joule heating method was used. This method easily supplies steady state heat flux and exhibits fast thermal response. Applied heat flux was calculated using the Joule's heat flux equation. (Eq. (1))

$$q'' = \frac{Power}{A_{heated}} = \frac{VI}{WL_{heated}} \quad (1)$$

Here, V is the measured voltage drop across the test material, I is the measure current, W is the width of the

heat transfer area, and L_{heated} is the heated length. Uncertainty of the measured heat flux was estimated as 5.2% based on the propagation of error method.

2.3 Test matrix

All the test surfaces used in this study are listed in Table 2. Here, *B* refers to 'bare', *Ox* refers to 'Oxidation', and *SP800* refers to 'ground with grade-800 sandpaper', respectively. For example, *Ox-SP320 (700C/3d)* refers to the test surface ground with grade-320 sandpaper and oxidized at 700 °C during 3 days.

Table 2. Test matrix

Surface condition	Oxidation at 500 °C during 10 days	Oxidation at 700 °C during 3 days
Bare	B-SP800	B-SP320
Ground with grade-800 sandpaper	Ox-SP800 (500C/10d)	Ox-SP800 (700C/3d)
Ground with grade-320 sandpaper	Ox-SP320 (500C/10d)	Ox-SP320 (700C/3d)

3. Result and discussion

3.1 Sample characterization

Fig. 2 shows the surface morphology of (a) B-SP800, (b) Ox-SP800 (500C/10d), and (c) Ox-SP320 (700C/3d). The vertical microscale scratches in Fig. 2(a) were caused by unidirectional grinding. As oxidation progressed, the oxide products were formed differently with oxidation condition. Lumped shape of oxide product was formed on Ox-SP800 (500C/10d) while oxides having a particulate nanostructure with hundreds of nanometer size were formed on Ox-SP800 (700C/3d).

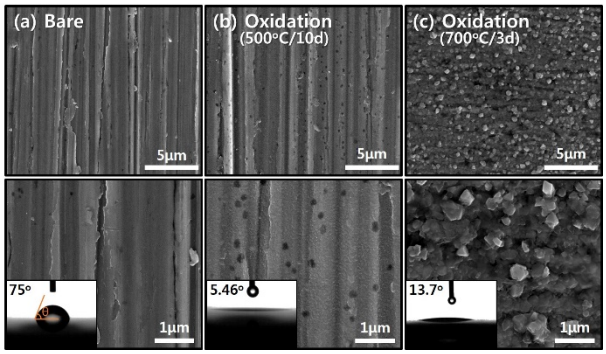

Fig. 2. SEM images of surface morphology: (a) B-SP800; (b) Ox-SP800 (500 C/10d); (c) Ox- SP800 (700 C/10d).

It is widely accepted that oxides make test surfaces superhydrophilic. We confirmed this here through contact angle (CA) measurement. The CA of the B-SP800 was 75°, whereas the CAs of the oxidized surfaces were very low, i.e., 5.46° on the Ox-SP800 (500C/10d) and 13.7° on Ox-SP800 (500C/10d).

3.2 Critical Heat Flux

Measured pool boiling curves are plotted in Fig. 3(a) and measured CHF are plotted in Fig. 3(b) after normalizing based on the result of B-SP800. Here, T_w is the temperature at the inner wall of test surface, measured by the attached thermocouple.

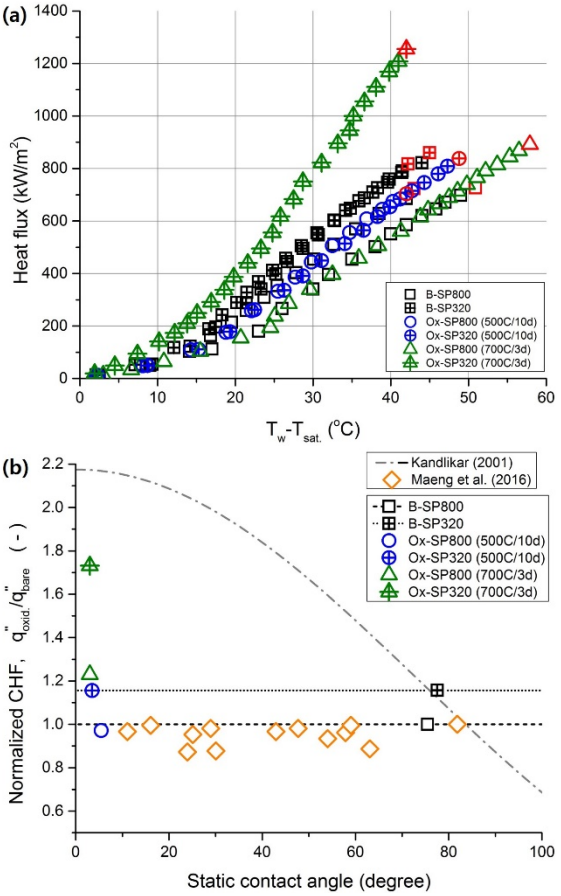

Fig. 3. (a) Pool boiling curves of the test surfaces (b) Normalized CHF of test surfaces following each static contact angle.

As shown in Fig. 3, an increase of surface roughness from B-SP800 to B-SP320 enhances CHF by 15.7%. In the case of the superhydrophilic oxidized surfaces, there was no significant enhancement on CHF with Ox-SP800 (500C/10d) and -SP320 (500C/10d) compared to each bare surfaces, which is B-SP800 and B-SP320, respectively. But the CHF of superhydrophilic Ox-SP800 (700C/3d) and Ox-SP320 (700C/3d) surfaces was enhanced by 23.0% and 49.7% each.

The measured CHF in this study was compared with Kandlikar's model in Fig. 3(b). Kandlikar's model covers the effect of the CA on the CHF. In this model, the predicted CHF, q_c'', enhanced following decrease of the contact angle, θ_r, as shown in eq. (2).

$$q_c'' = K \times h_{fg} \rho_g^{1/2} \left[\sigma_{lv} g \left(\rho_l - \rho_g \right) \right]^{1/4}$$
$$K = \left(\frac{1+\cos\theta_r}{16} \right) \left[\frac{2}{\pi} + \frac{\pi}{4} (1+\cos\theta_r) \cos\psi \right]^{1/2} \quad (2)$$

However, our result was not in good agreement with Kandlikar's CHF model because there was no meaningful enhancement in the CHF with superhydrophilic Ox-SP800 and –SP320 (500C/10d). Similar results were reported by Maeng et al., where they observed that the CHF of the various wettability improved surfaces sputtered by TiO_2 surfaces depending on the sputtering time were not enhanced meaningfully than that of bare surface although the wettability was maintained during the experiment. They claimed that it is because the time sputtering of TiO_2 was so short that any nanostructure was not built on the surface.

Likewise, the difference of the CHF enhancement between oxidation at 700 °C during 3 days and 500 °C during 10 days is due to the shape of the oxide products. As mentioned earlier, the particulate shape and the lumped shape were formed by oxidation at 700 °C during 3 days and 500 °C during 3 days, respectively. As shown in Fig. 2, oxide products of the lumped shape has no effect on the micro-scratch of the surfaces. Whereas, one of the particulate shape contributes the enhancement in the nanoscale roughness because the particulate shape oxide products enlarge the nanoscale surface area. In other words, the formation of the particulate nanostructure could contribute to enhancing the CHF. So, it is necessary to explore another parameter affecting the CHF because the CA did not affect the CHF unlike Kandlikar's CHF model.

3.3 Dynamic wetting

Recently, the researches to understand the pool boiling CHF mechanism have focused on the microlayer evaporation model. In this model, the liquid inflow sucked into the microlayer around dry spots delays the formation of dry patches. But with additional heat, the growth of dry spots dominates liquid inflow, which causes the formation of dry patches and eventually CHF. So, the enhancement of CHF, i.e. $q''_{enh.}$, by liquid inflow can be expressed as the following equation. (Eq. (3))

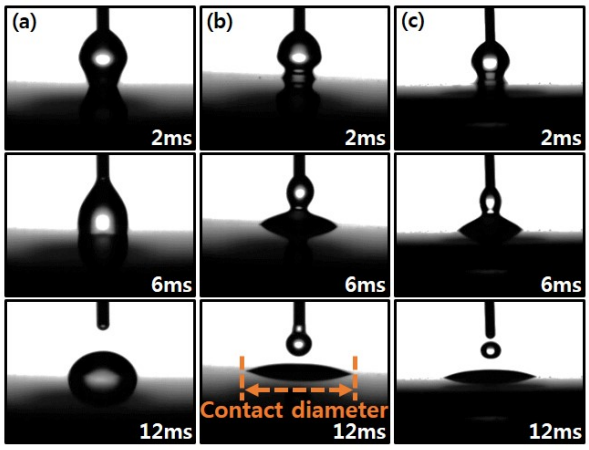

Fig. 4. High speed visualization of the spreading behavior on the test surfaces: (a) B-SP800; (b) Ox-SP800 (500 C/10d); (c) Ox-SP800 (700 C/3d).

$$q''_{enh.} = \frac{\dot{m}_f h_{fg}}{A_t} = \frac{\rho_f u_l A_c h_{fg}}{A_t} = B u_l \qquad (3)$$
$$B = \frac{\rho_f A_c h_{fg}}{A_t}$$

where $\dot{m}_f$ is the mass flux of liquid inflow, h_{fg} is the latent heat from liquid to gas, A_c and A_t is the cross-sectional area of microflow channel and the heat transfer area, ρ_f is the density of liquid, and u_l is the liquid inflow rate. Here, microflow channel refers to the micro-scratched lines on differently-ground test surfaces. If the microscale roughness was not changed, $\dot{m}_f$, h_{fg}, A_c, A_t, and ρ_f are constant. Consequently, the only parameter governing the enhancement of CHF by the liquid inflow is the liquid inflow rate.

Fig. 4 shows the spreading behavior of the water droplet on the test surfaces using the high speed camera, which is a sort of the dynamic wetting phenomenon. On B-SP800, the droplet formed the spherical shape on the bare surface, whereas the droplet spread over the oxidized surfaces. To quantify the liquid inflow rate from the images, we assumed that the liquid inflow rate was proportional to the advancing rate, u_a, of the water droplet, which refers to the slope of increasing liquid contact diameter at the interface between the droplet and the surface following spreading time.

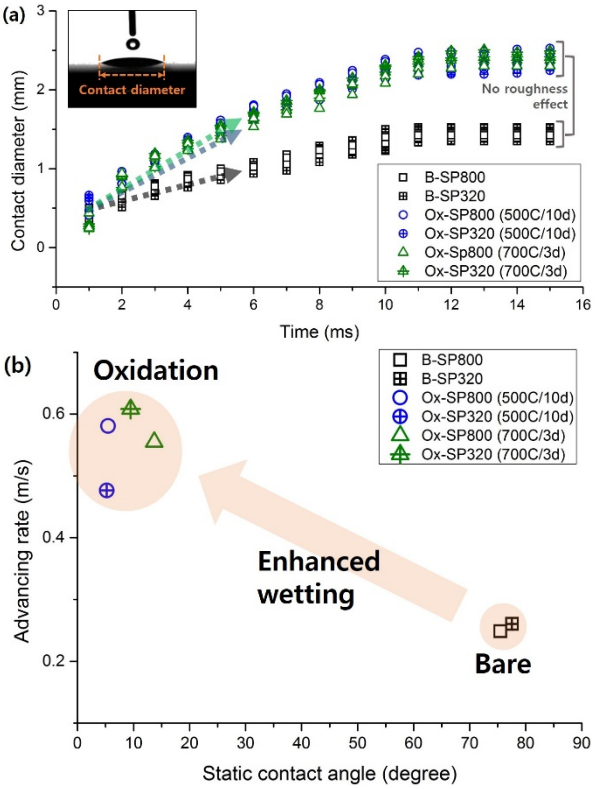

Fig. 5. Quantification of volumetric liquid inflow rate: (a) dynamic wetting behavior; (b) enhancement wettability due to the oxidation.

Fig. 5(a) shows the increasing contact diameter of each sample as a function of time. All of the contact diameters increased following the spreading time and converged in

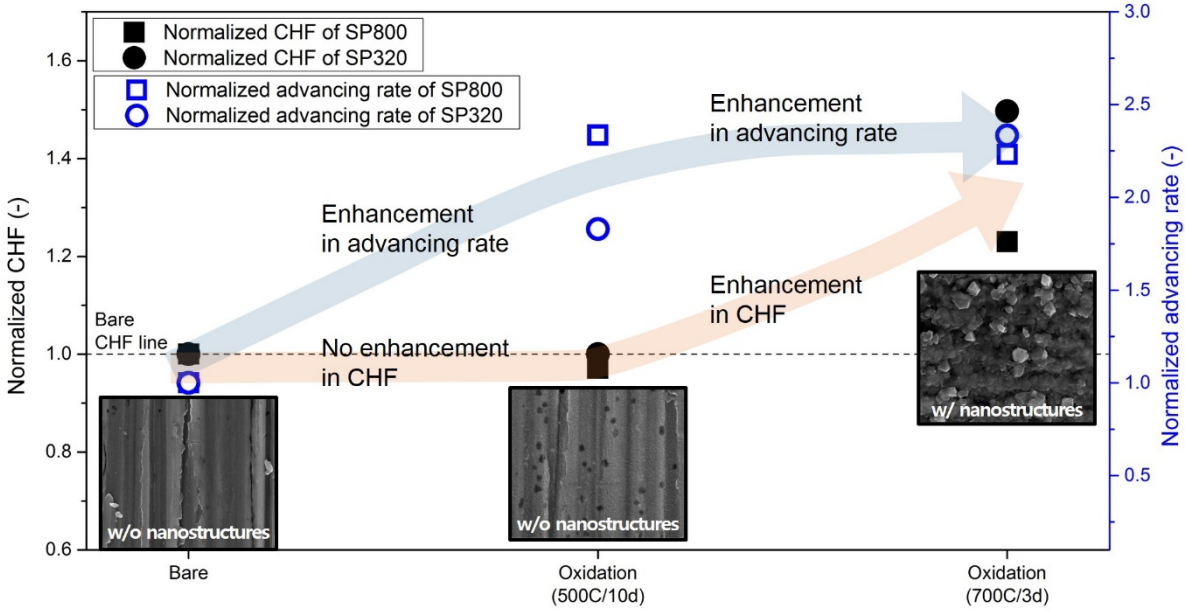

Fig. 6. Normalized CHF and advancing ratio of test surfaces.

a short time. There is the interesting phenomenon that the difference of the roughness between SP800 and SP320 didn't affect the advancing rate as shown in Fig. 5(a). It implies that the liquid spreading rate depends on nanostructures rather than micro-scratches. As oxidation enhanced the wettability of the test surfaces, advancing rates after the oxidation increased from 0.25 m/s for the bare surfaces to 0.52 m/s for 500 C/10d oxidized surface and 0.59 m/s for 700 C/3d oxidized surface, as shown in Fig. 5(b). Also, the oxidation decreased the CA of the test surfaces.

Fig. 6 shows normalized CHF and normalized advancing rate of the test surfaces. Both of CHF and advancing rate of the 700 ^{o}C & 3 days oxidized surfaces were enhanced compared to those of the bare surfaces. On the other hand, the normalized CHF did not enhance and the normalized advancing rate increased on the 500 ^{o}C & 10 days oxidized surfaces unlike the microlayer evaporation model. The reason of the difference between 700 ^{o}C & 3 days and 500 ^{o}C & 10 days is mainly the formation of the particulate nanostructure.

5. Conclusions

Pool boiling experiments were conducted with grade 304 stainless steel samples oxidized under two different conditions at 500 ^{o}C during 10 days and 700 ^{o}C during 3 days. After the oxidation, the effect of the dynamic wetting behavior on CHF enhancement with these oxidized surfaces was analyzed. According to the microlayer evaporation model, the advancing rate representing the dynamic wetting behavior was expected to show the similar enhancement of the CHF. However, some superhydrophilic oxidized surfaces resulted in the similarly increased advancing rate but the quite different enhancement in the CHF after the oxidation different from the microlayer evaporation model. We confirmed that the particulate nanostructure formed on metal oxides on the surface contributes to the enhancement on the CHF. So, the formation of the particulate nanostructure is needed to be considered as the CHF enhancement factors in addition to dynamic wetting behavior.

Acknowledgement

This research was supported by the National R&D Program through the National Research Foundation of Korea (NRF) funded by the Korean Government (MSIP: Ministry of Science, ICT and Future Planning) (No. NRF-2015R1C1A1A01054861) and by the National Research Foundation of Korea (NRF) grant funded by the Korean government (MSIP) (No. NRF-2016R1A5A1013919).

REFERENCES

[1] H.H. Son, U. Jeong, G.H. Seo, and S.J. Kim, Oxidation effect on the pool boiling critical heat flux of the carbon steel substrates, International Journal of Heat and Mass Transfer 93, 2016, 1008-1019.
[2] Y.H. Maeng, S.L. Song, J.Y. Lee, Unaffectedness of improved wettability on critical heat flux enhancement with TiO2 sputtered surface, Applied Physics Letters 108, 074101, 2016.
[3] H.W. Moon, Y.J. Yoon, J.H. Park, B.S. Myung, D.E. Kim, Dynamic wetting and boiling characteristics on micro-structured and micro/nano hierarchically structured surfaces, Experimental Thermal and Fluid Science 74, 2016, 19-26.